Laboratory Investigations into the Effects of Heating on Clay's Mechanical and Hydraulic Changes Using Geophysical Methods

Elizabeth Nunez[1]; Wing Shun Kwan, Ph.D., P.E., M.ASCE[2]; and Cesar Leal[3]

[1]Graduate Research Assistant, Dept. of Civil Engineering, California State Univ., Los Angeles. Email: enunez54@calstatela.edu
[2]Associate Professor, Dept. of Civil Engineering, California State Univ., Los Angeles (corresponding author). Email: wkwan4@calstatela.edu
[3]Graduate Research Assistant, Dept. of Civil Engineering, California State Univ., Los Angeles. Email: cleal5@calstatela.edu

ABSTRACT

This research explores the responses of reconstituted Kaolin clay samples due to simulations of wildfires in the laboratory using heat guns for control heating. Two laboratory geophysical methods, bender element and electrical resistivity, were used to detect the changes in soil's mechanical (shear modulus, G_{max}) and hydraulic properties (electrical resistivity, ρ) in real time, while soil specimens were heated, up to 60°C, to partially represent the temperatures in a wildfire. Measurements were compared with samples that had not been heated. Results show that the G_{max} values for the controlled samples were about 25% greater than those that were heated, which implied that heating causes soil strength reduction. Additionally, the electrical resistivity for the controlled samples was 55% higher than that of the heated samples, meaning that heating caused the kaolin specimens to be less permeable. Correlations between G_{max} versus temperature (T) and water content were developed. Results also allowed for the development of electrical resistivity, temperature, and water content correlations.

INTRODUCTION

Wildfires are one of the most common natural disasters California endures yearly. The damages above the ground surface are visible, with the destruction of the landscape. However, the damages done below the ground surface are not. Wildfires can significantly alter soil's hydro-mechanical properties, increasing the risk of geohazards that affect critical structures and putting lives at risk. Therefore, it is essential to study the effects of wildfire on soil from a geotechnical engineering standpoint to understand and better predict the consequences. Tragic post-wildfire events resulting from soil water repellency, like the 2018 Montecito mudslides after the Thomas fire, have motivated studies focusing on the effects of wildfires, or heat, on soil hydraulic and mechanical properties.

Previous studies have shown that water repellency increases in burnt soils, leading to more runoff. Doerr et al. (2004) investigated how soil water repellency is affected by heat in shallow (0-2.5 cm) soil samples from an Australian eucalypt forest heated between 250 °C and 400 °C then tested using the Water Drop Penetration Time method. The results show increased water repellency in all heated samples compared to unheated samples and indicated that heat intensity and duration significantly affect soil water repellency levels. Investigations after the 2018 Montecito by Kean et al. (2019) show a decrease in hydraulic conductivity in burned areas compared to the hydraulic conductivity of unburned areas. The study also compared their

findings to results from other investigations studying similar parameters in other mudslide events. Ultimately, the other investigations observed similar results, allowing Kean et al. (2019) to correlate the excess runoff triggering the mudslides due to the decrease in the soil's hydraulic conductivity.

Furthermore, the manifestation of shallow landslides after a wildfire in a mountainous terrain triggered the investigation of the effects of heat on soil strength because of its direct relation to slope stability. Cekerevac and Laloui (2004) used a triaxial setup capable of changing the confining liquid temperature. Specimens were tested at temperatures ranging from 5 ºC to 70 ºC, showing increases in shear strength and initial elastic moduli as temperature increases. Jaradat and Abdelaziz (2020) recently performed a similar testing procedure with similar results, indicating increased shear strength with temperature increase.

This investigation aims to quantify the electrical resistivity (ρ) and shear modulus (G_{max}) of reconstituted Kaolin clay samples exposed to a continuous change in temperature (heating and cooling) and compare them to values from non-heated control samples that dried at room temperature through cost-effective setups. Despite all the research performed, to the best of the authors' knowledge, no previous studies have used geophysical methods to determine the effects of wildfires or heat on soils in the laboratory. Using the small strain shear modulus (G_{max}), previous studies have shown a correlation between the undrained shear strength of soil and the shear wave velocity (V_s) through data from field testing (Andersen 2004; Dickenson 1994; L'Heureux and Long 2017). Additionally, investigations involving control lab testing (Black et al. 2009; Dyvik and Madshus 1985) had shown a linear relationship between undrained shear strength (S_u) and shear wave velocity (V_s) of soil from bender elements measurements. Similarly, in geophysical applications, electric resistivity, ρ, has been popular to measure how adequately sediments resist the flow of electric current. According to an investigation by Archie (1942), a proportionality exists between soil porosity and ρ of the pore water. Therefore, geotechnical engineering properties can be determined through electrical resistivity. Studies (Olabode and San 2023; Vogelgesang et al. 2020) have shown a potential correlation between electrical resistivity and hydraulic conductivity.

The correlation of electrical resistivity (ρ) and shear modulus (G_{max}) to the hydraulic conductivity and strength of the soil, respectively, can be helpful for soil parameter calibrations for a model that can aid the application of these non-invasive geophysical methods in the future. It can also help quantify the effects of wildfires in soils without the need for time-consuming invasive methods. This can lead to more effective post-wildfire assessments.

TESTING PROCEDURE

Reconstituted Kaolinite clay samples were used to carry out the experimental investigation. The Kaolinite, acquired from R.T. Vanderbitt Holding Company, Inc., falls within the CH group of the USCS, with plastic and liquid limits of 30% and 60%, respectively. The specimen reconstitution started with a slurry mixture of roughly 9 kilograms of clay and 10 kilograms of distilled water, followed by the consolidation of the mixture. A square stainless-steel box and a typical triaxial frame were used for consolidation (Figures 1A and 1B) following the method of slurry-based consolidation (Suzuki and Dyvik 2017) and a staged consolidation schedule at incremental stress levels of 5 kPa, 12.5 kPa, 25 kPa, and 50 kPa, as documented in (Kam et al. 2020). Sample retrieval followed the completion of the consolidation phase, using four 7.1 cm diameter Shelby tubes inserted into the consolidated clay (Figure 1C). Excess clay was

trimmed and removed to expose the Shelby tubes (Figure 1D). After sample retrieval and labeling, they were stored under moisture control conditions. For the six specimens that were tested in this study, the water content range is 50% to 62% (average = 55.6%, one standard deviation = 5.2%).

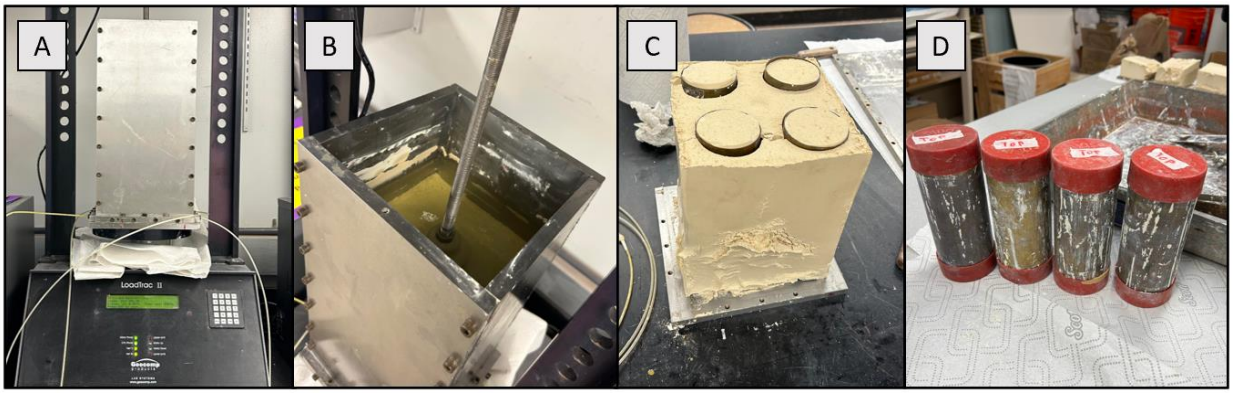

Figure 1. Kaolin Specimen Preparation: (A) Consolidation box, (B) During Consolidation, (C) Consolidated Kaolin Block after Disassembling the Consolidation Box, and (D) Cored and Trimmed Samples

The bender element and electrical resistance setups were placed on a digital scale to track the sample's change in weight during the heating and cooling cycle (Figures 2A & 3A). As a result, the change in water content can be quantified by assuming no soil mass losses and correlating the change in soil weight to the evaporation of pore water. Additionally, a dial gauge was placed in contact with the top cap to keep track of height changes, allowing researchers to track the changes in the sample's density during the test. A thermocouple was inserted into the upper and lower half of the specimen to track temperature during the heating and cooling cycle. Temperature readings from the top and bottom of the specimen were monitored throughout the tests, and the specimen's temperatures were calculated by the average of the two. Geophysical testing enables real-time measurements at various temperatures for one soil specimen; however, traditional methods like standard triaxial or permeability tests to investigate heating effects may require multiple specimens at different temperatures. A crucial benefit of this setup is that nothing, including the soil specimen and instrumentations, was disturbed except changing temperatures in the heat guns. The testing was set up with commonly available equipment, allowing tests to be repeated by many other geotechnical laboratories.

The heating's goal was for the soil's temperature to reach as high and quickly as possible to simulate wildfire. Figures 2A and 3A show that two Wagner Furno 700 heat guns were used to heat samples. The heat guns were pointed to the center of the specimen and constantly adjusted to ensure the top and bottom of the sample experienced the same degree of heat. However, due to the limitations of the testing equipment, the highest possible temperature was around 60 °C at a rate of 6 ºC per hour. A higher temperature and heating rate were desired to simulate wildfires better. However, from experience, a higher heating rate resulted in the clay cracking and breaking off from the Shelby tube. Equipment limitations also prevented reaching higher temperatures. After reaching 60 ºC, the noise levels from the bender element and electricity resistivity devices had become too high to process, indicating the non-heat-proof apparatus could not endure further elevated temperatures, forcing the end of the heating phase to move into the

cooling stage under room temperature (20.5 ºC) at an exponential rate of -0.3 ºC per hour while continuously taking measurements of G_{max} or ρ until the sample temperature was near to room temperature.

The specific setup for the bender element testing is shown in Figure 2A. Samples were stationed on a laboratory stand, and shear wave velocity (V_s) was measured during the heating and cooling cycle to capture the changes in the clay's stiffness. On average, 33 measurements were taken for the heating-cooling tests that were 6-8 hours long. Throughout the testing, the frequency of the wave generator was adjusted until the receiving wave, recorded from the top cap, was clear and had a similar period to the triggered wave generated at the bottom cap (Figure 2B). The response time of the wave passing through the test specimen was recorded from the triggered wave's first peak to the arrival wave's first peak following ASTM D8295-19. The V_s value was then calculated by dividing the height of the specimen by the response time. G_{max} can then be calculated by using the following:

$$G_{max} = \rho_T V_s^2$$

where ρ_T is the density of the specimen.

Figure 3A shows the specific setup for the electrical resistivity testing, with samples mounted on a modified trimmer. For the duration of the heating and cooling cycle (6-8 hours), the electrical resistance (R) was measured by an analog resistance meter (Miller 400 A), along with the changes in dial gauge, temperature, weight, and time. Kwan et al. (2019) documents the details of the apparatus (Figure 3B) and its usages in real-time triaxial testing. Additional vertical stress (12 kPa) was kept on the vertical alignment to ensure a better contact surface between the electrical conductors and the soil surface. Electrical resistivity, ρ, is calculated from electrical resistance (R) using the equation below:

$$\rho = R * \frac{A}{L}$$

where L is the specimen height, and A is the cross-sectional area.

Controlled (unheated) tests were necessary to see the effects of heat on the shear modulus and electrical resistivity of the soil in terms of magnitude and rate of change. The controlled testing lasted 3-4 weeks, in which both bender element and electrical resistance samples experienced no heating, allowing them to dry at room temperature. Using the previously mentioned processes, measurements (e.g., specimen's weight, temperatures, height, and R or V_s) were taken almost daily as the specimen was kept at room temperature. About 30 measurements were taken throughout the 3-4 weeks.

After concluding the control or heating-cooling testing, the sample was oven-dried to calculate the final water content $(w.c.)_f$. Since the heating procedure involved heat guns pointing to the middle portion of the specimen, heterogeneous distributions of pore water along the sample were expected. Therefore, instead of a typical water content test considering only a portion of soil mass, the entire sample was oven-dried to capture the global water content. The water content of the specimen at any given time or temperature during testing was back calculated using the final water content along with the change in water mass. The $(w.c.)_f$ values are summarized in Table 1.

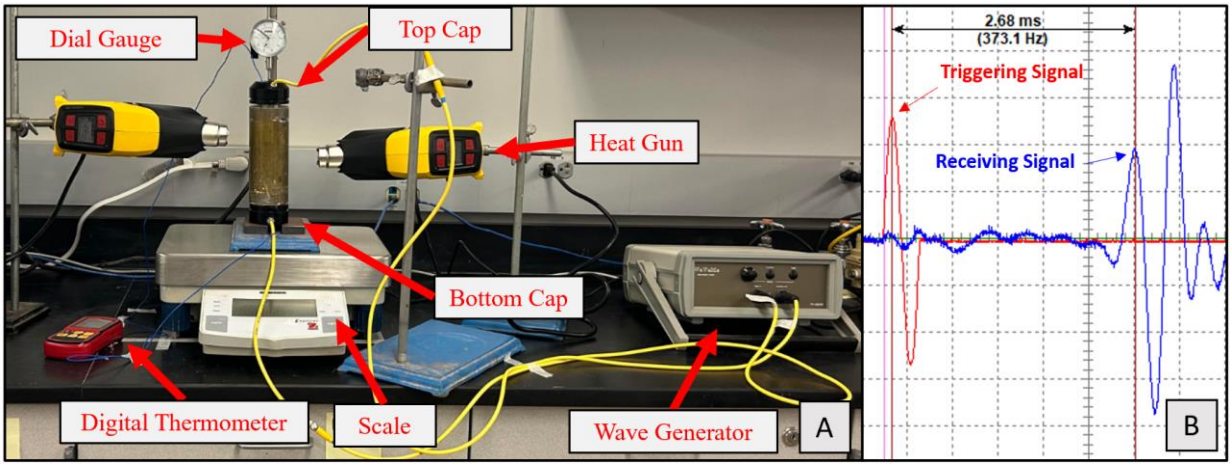

Figure 2. (A) G_{max} Setup, and (B) – A Demo of Time Difference between the Triggering and Arrival Signals during a Bender Element Test

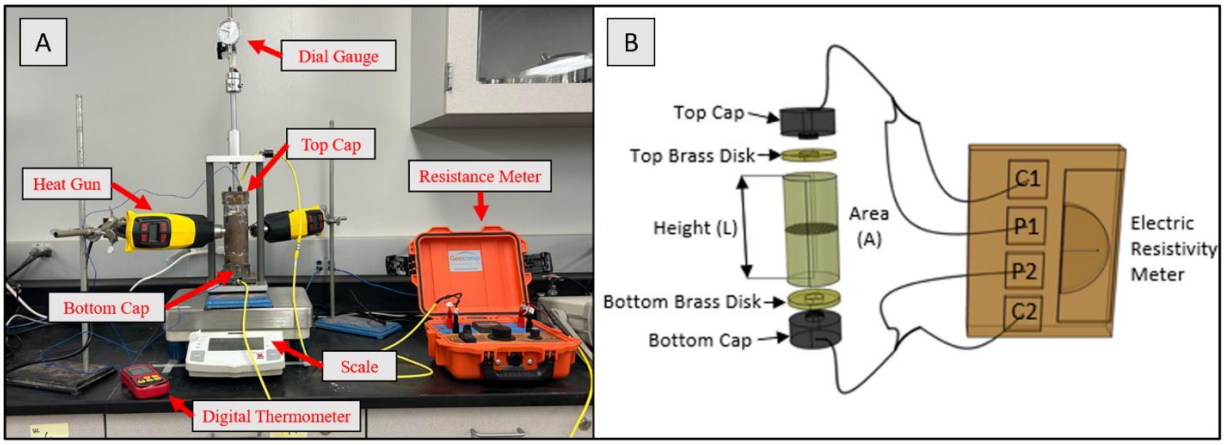

Figure 3. (A) Electrical Resistivity Setup, and (B) Schematic Sketch of Electrical Resistivity Triaxial Caps and the Miller 400A Resistance Meter (Kwan et al. 2019)

DATA

The table shown below is a summary of the data obtained during testing. The bender element tested samples are named "B" followed by a "CON" or "HC" depending on whether it was a controlled test or if it involved heating and cooling. If there is a number at the end, then that signifies that multiple samples had the same testing procedure. Resistivity-tested samples have the same naming format, but an "R" is used in place of the" B." Trials were repeated (HC1 and HC2) to ensure that results can be repeated by anyone conducting the same test. Tests B-HC2 and R-HC2 were given an extra day to return to room temperature. Therefore, their final temperatures are 24.5 ºC and 21.3 ºC, respectively, versus 28.7 ºC and 26.8 ºC from B-HC1 and R-HC1.

Table 1. Summary of Test Results

Test ID	$(w.c.)_i$ (%)	$(w.c.)_f$ (%)	$(mass)_i$ (g)	$(mass)_f$ (g)	Temp. (°C)	G_{max} (MPa)	Electrical Resistivity (Ω·m)
B-CON	60.4	46.6	744.2	686	21.3-22.7	7.6-42.9	-
B-HC1	59.4	45.6	737	673.3	21.6-59.1	4.8-38.7	-
B-HC2	51	40.7	749.6	698.9	22.3-59	4.7-31.8	-
R-CON	62.3	42.4	737.8	646.9	20.5-22.5	-	85.8-319.2
R-HC1	49.7	42.3	732	696.2	21.7-58.9	-	59.6-117.1
R-HC2	50.7	37.5	740.15	674.5	21.3-61	-	61-166.6

RESULTS AND DISCUSSION

Figures 4 and 5 depict the evolutions of shear modulus, electrical resistivity, and density values while the six samples were subjected to heating and cooling or drying at room temperature.

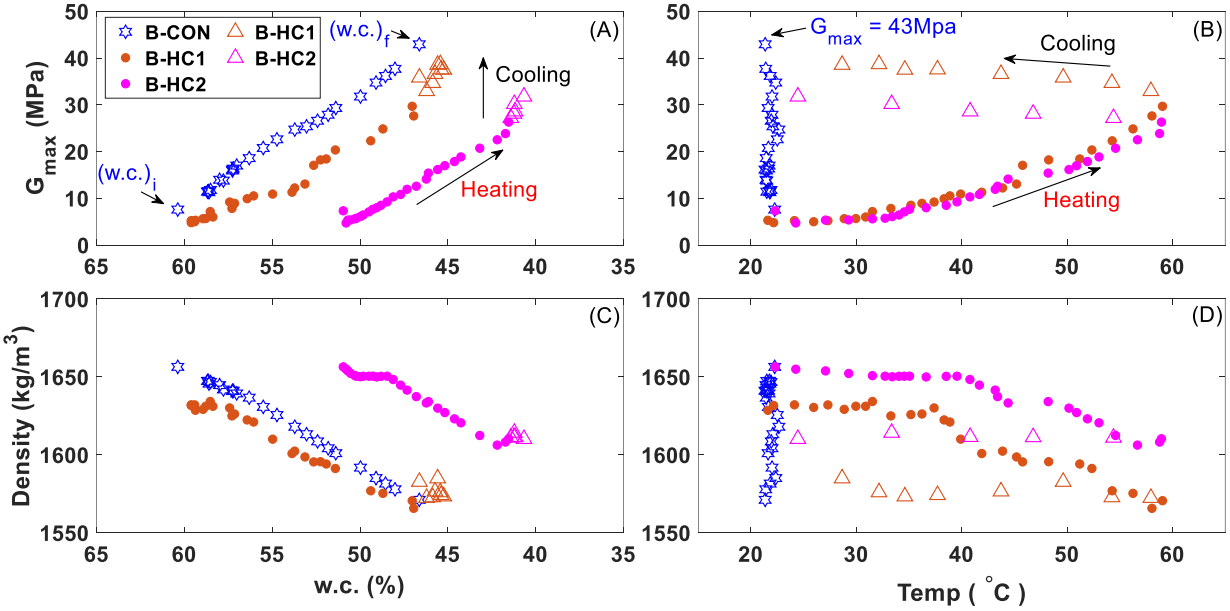

Figure 4. (A) G_{max} vs Water Content (solid dots = heating; open triangles = cooling), (B) G_{max} vs Temperature, (C) Density vs. Water Content, and (D) Density vs. Temperature

- Figure 4A: In both heated and non-heated samples, the G_{max} increases linearly as the clay samples dry out (i.e., decrease in water content). The controlled test, B-CON, experienced an increase in shear modulus at a rate of 2.42 MPa/%w.c. while the heated tests, B-HC1 and B-HC2, experienced a rise in G_{max} at a rate of 1.82 MPa/%w.c. and 2.14

MPa/%w.c. respectively. B-HC1 and B-HC2 had G_{max} increase rates during cooling (open triangles) that were 1.6 and 2.7 times faster, respectively, than during the heating phase.

- Figure 4B: B-HC1 and B-HC2 show almost identical G_{max} exponential growth rates, driven by the exponential growth of shear wave velocity, with an average of .049 MPa per ºC during the heating phase and .005 MPa per ºC during the cooling phase. For the control test, B-CON, the sample remained constant at 21 ºC. Results from B-HC1 are comparable with those from B-HC2, showing the repeatability of the G_{max} testing procedures.
- Figure 4C: The total densities of the three tests linearly decreased at an almost identical linear rate, where the average linear rate for B-HC1 and B-HC2 was 5.35 kg/m^3 per %w.c, and the linear rate for B-CON 6.5 kg/m^3 per %w.c. showing that heating did not affect the water evaporation in the absence of time. It was noticed that the densities remained constant during the cooling period for B-HC1 and B-HC2. However, for the control test, B-CON, the density kept decreasing with the decrease in water content.
- Figure 4D: The total densities of B-HC1 and B-HC1 decrease with the temperature increase at an average linear rate of 1.6 kg/m^3 per ºC. Once the heated samples began the cooling phase, temperatures decreased while densities remained constant. For B-CON, the specimen's density decreases without a temperature change.

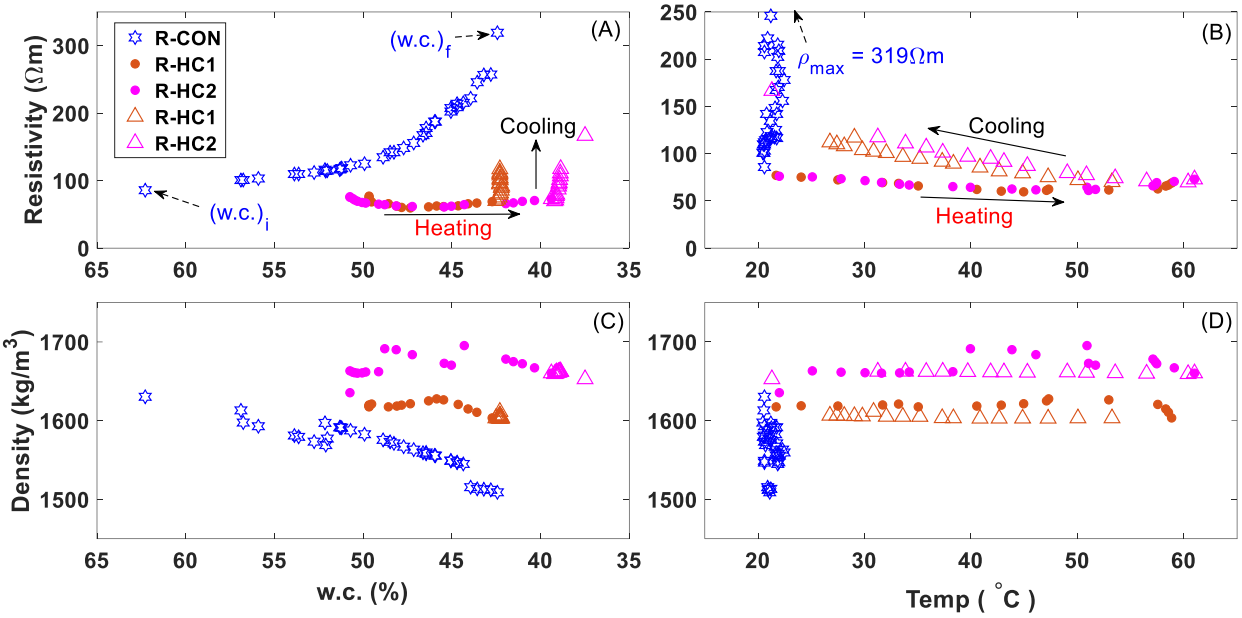

Figure 5. (A) Electrical Resistivity vs Water Content (solid dots = heating; open triangles = cooling), (B) Electrical Resistivity vs Temperature, (C) Density vs. Water Content, and (D) Density vs. Temperature

- Figure 5A: Before heating, ρ values from R-HC1 and R-HC2 are similar to the values from R-CON. However, R-CON had a much faster rate of increase (exponential growth rate of .067 Ω-m/%w.c.) in ρ as the sample was drying out. R-HC1 and R-HC2 show little to no change in electrical resistivity until the cooling phase. Once reaching the

cooling phase, the two R-HC tests showed a sharp increase in resistivity while the water content stayed relatively the same. At the end of the tests, R-HC tests only reach around half of the ultimate ρ value from the R-CON test at similar or lower water contents.

- Figure 5B: R-HC1 and R-HC2 again show little to no change in ρ during the heating phase while the temperature increases. On the contrary, during the cooling phase, as temperature goes back to room temperature, resistivity slightly increases at an exponential rate of .021 per °C. After the cooling stage, the final ρ value of R-HC2 was 166.67 Ω-m, while the final resistivity value for R-CON was 319.21 Ω-m. Additionally, R-HC2 achieved a lower final water content of 37.5% than 42.4% of R-CON. The cooling phase did not show a full recovery in ρ. Results from R-HC1 are comparable with those from R-HC2, showing the repeatability of our electrical resistivity testing procedures.
- Figure 5C: R-HC1 and R-HC2 have little to no change in density as the water content drops. However, R-CON shows a decrease in density with the decline of water content with a linear rate of 5.6 kg/m^3 per %w.c.
- Figure 5D: Similarly, in tests R-HC1 and R-HC2, there is little to no change in density when temperatures change, while R-CON had a steady decrease in density at a constant temperature. A higher vertical stress (12 kPa) was applied to the electrical resistivity specimens compared to the bender element specimens (2.6 kPa, weight of the top cap); therefore, less change in density was recorded compared to Figure 4D.

Using the Polyfit application in Matlab, results for G_{max} and ρ were fitted with their respective temperature and water content to the first, second, and third degree to determine correlations to better predict soil strength (G_{max}) and hydraulic conductivity (ρ). Table 2 shows the correlation coefficient (R^2 value) of G_{max} vs. w.c. ($R^2 > 0.98$) are very similar to G_{max} vs. T ($R^2 > 0.98$), indicating that both w.c. and T are good predictors of soil strength. Water content is a good predictor of G_{max} with or without temperature changes. From Table 3, the R^2 values of (ρ vs. w.c.) are lower than the R^2 values of (ρ vs. T). Results show that temperature is a better predictor of electrical resistivity than water content.

Table 2. Polynomial Fittings for G_{max} vs. Water Content vs. Temperature

		Degree		
Test	**R^2**	**w.c.**	**T**	**Equation, G_{max} =**
B-CON	0.994	1	-	-2.42(w.c.)+154.13
	0.994	1	1	163.59-2.43(w.c.)-0.43(T)
	0.997	2	2	1886-5.02(w.c.)-151(T)-0.02 $(w.c.)^2$+0.22(w.c.)(T)+3.16$(T)^2$
B-HC1	0.987	2	-	0.10$(w.c.)^2$-13.11(w.c.)+418.84
	0.989	-	2	0.02$(T)^2$-0.73(T)+12.8
	0.984	1	1	161.66-2.55(w.c.)-0.22(T)
	0.991	2	2	504.64-16.04(w.c.)-0.54(T)+0.13 $(w.c.)^2$+0.014(w.c.)(T)-0.0022$(T)^2$
B-HC2	0.987	2	-	0.10$(w.c.)^2$-11.66(w.c.)+337.04
	0.986	-	2	0.02$(T)^2$-0.73(T)+12.8
	0.994	1	1	144.88-2.68(w.c.)-0.15(T)
	0.994	2	2	49.76+1.13(w.c.)+0.45(T)-0.037 $(w.c.)^2$-0.13(w.c.)-.000524$(T)^2$

Table 3. Polynomial Fittings for Resistivity vs. Water Content vs. Temperature

		Degree		
Test	**R^2**	**w.c.**	**T**	**Equation, ρ =**
R-CON	0.984	3	-	$-0.07(w.c.)^3+11.99(w.c.)^2-670.12(w.c.)+12607$
	0.824	1	1	$1221-11.88(w.c.)-22.54(T)$
	0.958	2	2	$648.6-61.48(w.c.)+140.6(T)+0.74\ (w.c.)^2-1.18(w.c.)(T)-2.26(T)^2$
R-HC1	0.650	3	-	$-0.30(w.c.)^3+42.73(w.c.)^2-2047.8(w.c.)+32699$
	0.916	-	2	$0.029(T)^2-2.65(T)+122.86$
	0.945	1	1	$335.93-4.61(w.c.)-1.26(T)$
	0.987	2	2	$2667-97.3(w.c.)-14.75(T)+0.93(w.c.)^2+0.23(w.c.)(T)+0.04(T)^2$
R-HC2	0.630	3	-	$-0.08(w.c.)^3+11.36(w.c.)^2+538.62(w.c.)+8527.4$
	0.885	-	1	$0.031(T)^2-2.81(T)+126.06$
	0.912	1	1	$329.07-4.12(w.c.)-1.65(T)$
	0.996	2	2	$1410-45.1(w.c.)-12.8(T)+0.39\ (w.c.)^2+0.19(w.c.)(T)+0.04(T)^2$

CONCLUSION

This study aimed to determine how the mechanical and hydraulic properties of Kaolin clay were affected due to controlled heating under limitations of the temperatures of the heated samples, which only went up to 60 ºC. This research only reached a fraction of the temperature wildfires can typically reach. However, even at such a small scale, hydraulic conductivity and soil strength decreased in the heated samples compared to the unheated ones. It can be inferred that the soil hydraulic impedance and strength reduction will only worsen when temperatures reach anywhere near those during wildfires. At the end of the cooling period of the heated samples, the final electrical resistivity values are only about half of the final value from the unheated test, showing there may not be a full recovery in infiltration after heating. From the bender element tests, heated samples recorded final G_{max} values about 25% less than the final value from the unheated test, showing there were likely strength losses on soils after experiencing a wildfire event. Further testing with better heat-resistant testing equipment is needed to better understand these changes' magnitude.

ACKNOWLEDGMENT

This work has been supported by the National Science Foundation with Award No. HRD-2112554. Elizabeth Nunez and Cesar Leal are recipients of the CREST-CATSUS fellowship, for which we are grateful.

REFERENCES

Andersen, K. H. (2004). “Cyclic clay data for foundation design of structures subjected to wave loading.” *International Conference on Cyclic Behaviour of Soils and Liquefaction Phenomena*, 3133–3234. Bochum, Germany.

Archie, G. E. (1942). “The Electrical Resistivity Log as an Aid in Determining Some Reservoir Characteristics.” *Transactions of the AIME*, 146: 54–62.

ASTM D8295-19. (2019). *Standard Test Method for Determination of Shear Wave Velocity and Initial Shear Modulus in Soil Specimens using Bender Elements*. West Conshohocken, PA.

Black, J. A., S. A. Stanier, and S. Clarke. (2009). "Shear wave velocity measurement of kaolin during undrained unconsolidated triaxial compression." *62nd Canadian Geotechnical Conference*, 20–23. Halifax, Canada.

Cekerevac, C., and L. Laloui. (2004). "Experimental study of thermal effects on the mechanical behaviour of a clay." *Interntaional Journal for Numerical and Analytical Methods in Geomechanics*, 28 (3): 209–228.

Dickenson, S. E. (1994). *Dynamic Response of Soft and Deep Cohesive Soils during the Loma Prieta Earthquake of October 17, 1989*. University of California, Berkeley.

Doerr, S. H., W. H. Blake, R. A. Shakesby, F. Stagnitti, S. H. Vuurens, G. S. Humphreys, and P. Wallbrink. (2004). "Heating effects on water repellency in Australian eucalypt forest soils and their value in estimating wildfire soil temperatures." *International Journal of Wildland Fire*, 13 (2): 157–163.

Dyvik, R., and C. Madshus. (1985). "Lab Measurement of Gmax Using Bender Elements." Advances in the Art of Testing Soils Under Cyclic Conditions. New York: ASCE.

Jaradat, K. A., and S. L. Abdelaziz. (2020). "Thermomechanical triaxial cell for rate-controlled heating-cooling cycles." *Geotechnical Testing Journal*, 43 (4). ASTM International.

Kam, T., W. S. Kwan, M. Tufenkjian, and J. Fuentes. (2020). "Predicting Soil Strength using Electrical Resistivity Measurements in Clays." *GeoVirtual - Resilience and Innovation*.

Kean, J. W., D. M. Staley, J. T. Lancaster, F. K. Rengers, B. J. Swanson, J. A. Coe, J. L. Hernandez, A. J. Sigman, K. E. Allstadt, and D. N. Lindsay. (2019). "Inundation, flow dynamics, and damage in the 9 January 2018 Montecito debris-flow event, California, USA: Opportunities and challenges for post-wildfire risk assessment." *Geosphere*, 15 (4): 1140–1163.

Kwan, W. S., M. Tufenkjian, J. Tuazon, N. Peralta, K. Khov, and F. Garcia. (2019). "Electrical Resistivity Measurements in Advanced Triaxial Tests." *Geo-Congress 2019: Eighth International Conference on Case Histories in Geotechnical Engineering*. Philadelphia.

L'Heureux, J.-S., and M. Long. (2017). "Relationship between Shear-Wave Velocity and Geotechnical Parameters for Norwegian Clays." *Journal of Geotechnical and Geoenvironmental Engineering*, 143 (6): 04017013.

Olabode, O. P., and L. H. San. (2023). "Analysis of soil electrical resistivity and hydraulic conductivity relationship for characterization of lithology inducing slope instability in residual soil." *International Journal of Geo-Engineering*, 14 (1). Springer.

Suzuki, Y., and R. Dyvik. (2017). "Comparisons of Two Reconstitution Methods for Clay Specimens." *Geotechnical Frontiers 2017: Geotechnical Materials, Modeling, and Testing (GSP 280)*, 347–357.

Vogelgesang, J. A., N. Holt, K. E. Schilling, M. Gannon, and S. Tassier-Surine. (2020). "Using high-resolution electrical resistivity to estimate hydraulic conductivity and improve characterization of alluvial aquifers." *Journal of Hydrology (Amst)*, 580. Elsevier B.V.